Soft Matter

PAPER

View Article Online
View Journal | View Issue

Check for updates

Cite this: *Soft Matter*, 2019, **15**, 4146

Miniaturised acoustofluidic tactile haptic actuator

Asma Akther,[a] Jasmine O. Castro,[a] Seyed Ali Mousavi Shaegh,[bc] Amgad R. Rezk*[a] and Leslie Y. Yeo[a]

Tactile haptic feedback is an important consideration in the design of advanced human–machine interfaces, particularly in an age of increasing reliance on automation and artificial intelligence. In this work, we show that the typical nanometer-order surface displacement amplitudes of piezoelectric transducers—which are too small to be detectable by the human touch, and constitute a significant constraint in their use for tactile haptic surface actuation—can be circumvented by coupling the vibration into a liquid to drive the deflection of a thermoplastic membrane. In particular, transmission of the sound energy from the standing wave vibration generated along a piezoelectric transducer into a microfluidic chamber atop which the membrane is attached is observed to amplify the mechanical vibration signalling through both the acoustic radiation pressure and the viscous normal stress acting on the membrane—the latter arising due to the acoustic streaming generated as the sound wave propagates through the liquid—to produce 100 μm-order static deflections of the membrane, upon which approximately 0.5 μm dynamic vibrations at frequencies around 1 kHz are superimposed; both these static and dynamic responses are within the perception range for human finger sensation. The large static deformation, the relatively fast response time, and the ability to incorporate a dynamic vibrotactile response together with the small size and potential for integration of the device into large scale arrays make this mechanism well suited for driving actuation in devices which require tactile haptic responses.

Received 7th March 2019,
Accepted 13th April 2019

DOI: 10.1039/c9sm00479c

rsc.li/soft-matter-journal

Published on 15 April 2019. Downloaded by RMIT University Library on 5/18/2021 12:58:18 AM.

Introduction

The human sensory function is central to our interactions with the surrounding environment. The growth not just in our reliance on modern machines but also in their corresponding complexity has therefore necessitated the development of increasingly sophisticated human–machine interfaces that enhance our experience during their use, and, in many instances, our ability to use them more effectively. While these interfaces have primarily been focused on facilitating feedback *via* visual and auditory cues, there is an increasing emphasis on the development of tactile haptic devices that artificially create the sensation of touch through pressure, shear or vibration as a feedback mechanism to the user, particularly for interactive computing, flight/vehicle simulators, mobile phones, remote surgical instrumentation and robotics.[1–3]

Haptic surfaces, for example, can be controlled to arbitrarily deform as a means of transferring tactile information *via* localised stimuli to sensitive mechanoreceptors in the skin. Various mechanisms can be used to drive such deformation of a variety of materials, including different types of polymer[4–6] and elastomer[7,8] films, through the use of pneumatic,[9,10] electrostatic[5,7] and piezoelectric[11] actuators, among others. Pneumatic platforms can provide large displacement and hence impressive force feedback, but require large auxiliary equipment such as pumps and fans that make integration into portable consumer devices difficult. Electrostatic displacement schemes, on the other hand, usually require large kV order potentials which render them potentially hazardous for certain applications.[5,7] In addition, these schemes suffer from poor displacements (typically tens of microns).[5,12] Piezoelectric actuators, in contrast, are typically small in size (with chips on the millimeter scale), require significantly lower input voltages and offer the possibility for precise displacement tunability since the surface vibration can be localised. Nevertheless, the displacement magnitude that can be achieved with these actuators, especially when triggered at MHz order frequencies, has traditionally been limited to several tens of nanometers at best.[11]

In this work, we attempt to exploit these advantages of piezoelectric actuators, namely, their small size, low voltage requirement, and ability to tune the displacement they generate,[13] but also circumvent their limitations by coupling the vibration, *i.e.*, the sound energy, into a liquid phase in order to simultaneously provide a vibrotactile response as well as achieve a displacement

[a] *School of Engineering, RMIT University, Melbourne, VIC 3001, Australia. E-mail: amgad.rezk@rmit.edu.au*
[b] *Orthopedic Research Center, Mashhad University of Medical Sciences, Mashhad, 9176699199, Iran*
[c] *Clinical Research Unit, Mashhad University of Medical Sciences, Mashhad, 9176699199, Iran*

This journal is © The Royal Society of Chemistry 2019

Published on 15 April 2019. Downloaded by RMIT University Library on 5/18/2021 12:58:18 AM.

magnitude that is sufficiently large for the requirements of both static (≈100–200 μm) and dynamic (≈0.1 μm in the sub-kHz to 1 kHz frequency range) feedback.[14–17] We also show that the platform can, in principle, be parallelised into an array and integrated onto a printed circuit board (PCB) for use in a mobile phone or for haptic Braille perception (*e.g.*, V-Braille) wherein device portability and mobility are critical design specifications.

Experimental setup

A schematic depicting the conceptual set-up of the proposed haptic device is shown in Fig. 1 in which a 1.1 mm-high liquid chamber, fabricated by micro-machining a through-hole of varying inner diameter (2–5 mm) in poly(methyl methacrylate) (PMMA; GF13025652, Sigma-Aldrich Pty. Ltd, Castle Hill, NSW, Australia), chosen due to its lower rate of acoustic energy absorption compared to other soft materials such as poly(dimethylsiloxane) (PDMS),[18] was bonded using pressure-sensitive adhesive (OCA8146; Thorlabs, Newton, NJ) onto a 1 mm-thick 20 mm-diameter double-side aluminium-coated lead zirconium titanate (PZT; SOAR Piezo, Guangdong, China) disc. The inner walls of the chamber were hydrophobically coated (NeverWet; Rust-Oleum, Vernon Hills, IL) and subsequently filled with a 50 : 50 wt% mixture of water and glycerol (77067; Sigma-Aldrich Pty. Ltd, Castle Hill, NSW, Australia) and confined from above by a 25 μm- or 100 μm-thick flexible and transparent circular thermoplastic polyurethane (TPU, PT9200; Covestro Pty. Ltd, Cheltenham, VIC, Australia) membrane, cut from a sheet using a hole puncher to match the dimensions of the PMMA chamber and bonded along the 2 mm-thick peripheral walls of the chamber using the same pressure-sensitive adhesive (parenthetically, we note that the transparency of both TPU and PMMA makes them attractive materials particularly for display applications). We elected to use this method of bonding over the conventional method of high-temperature (60–80 °C) vacuum bonding,[19,20] as we found the latter to weaken the membrane, resulting in low durability, for this particular application, particularly over prolonged exposure to the vibration that resulted in leakage of the fluid. Moreover, the adhesive allowed us a fast (1–2 seconds, as opposed to 32 hours with high-temperature vacuum bonding) and easy way of bonding the materials. Prior to bonding, we ensured that no air bubbles were trapped between the liquid and the membrane *via* visual inspection under a microscope and high speed camera, and that the membrane was, as a starting point prior to the sound wave excitation (Fig. 1a), as flat as possible. Conceptually, the actuator is then potentially able to induce a tactile sensation to a human finger (as depicted in Fig. 1b) when a long burst of AC voltage is applied to the piezoelectric substrate (Fig. 1c).

Bulk waves were excited through the thickness of the PZT disc by applying a sinusoidal electric signal with an input voltage range between 24 and 54 V_{pp} at its resonant frequency (6.9 MHz), as measured using a vector network analyser (ZNB 4, Rohde & Schwarz, North Ryde, NSW, Australia) in Fig. 1d, using a signal

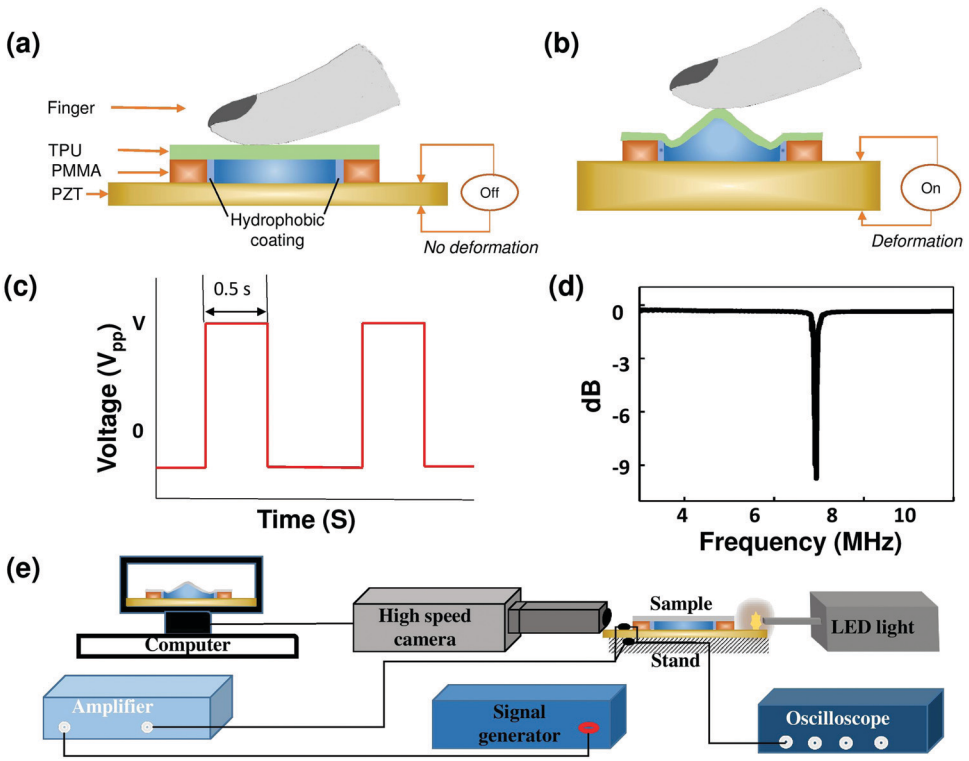

Fig. 1 (a and b) Side view schematics of the acoustofluidic actuator platform comprising a glycerol/water solution confined within a PMMA liquid chamber that is enclosed at the bottom by a PZT disc and at the top by a TPU membrane for generating tactile haptic feedback. Bulk waves are excited in the PZT disc upon (c) application of an AC electrical pulse in order to drive the membrane deformation. (d) Insertion loss parameter S_{11}, as measured through a frequency sweep using a vector network analyser, showing the resonant frequency of the PZT disc at 6.9 MHz. (e) Experimental set-up employed to measure the mechanical response of the membrane under the imposed vibration.

Published on 15 April 2019. Downloaded by RMIT University Library on 5/18/2021 12:58:18 AM.

generator (N9310A, Keysight Technology Pty. Ltd, Mulgrave, VIC, Australia) and RF amplifier (Electronics & Innovation Ltd, West Henrietta, NY, USA) (Fig. 1e). To monitor the current and voltage, we employed current (P6022, Tektronix, Beaverton, OR) and voltage probes with a 10:1 built-in attenuator (ZP10, Rohde & Schwarz, North Ryde, NSW, Australia) connected to an oscilloscope (RTM 1054; Rohde & Schwarz, North Ryde, NSW, Australia). The vibration displacement amplitude along the PZT, typically between 1.3 and 3 nm, was measured in the absence of the liquid loading using a laser Doppler vibrometer (LDV, UHF-120; Polytec Inc., Irvine, CA). The dynamic deflection of the TPU membrane was then measured with the LDV as well as observed using a high speed camera (SA5; Photron Ltd, Tokyo, Japan) at frame rates between 4 and 9.3 kfps connected to a telescopic lens (K2 with CF-4 objective; Edmund Optics Inc., Barrington, NJ) under LED illumination (RS-232, Nathaniel Group Inc., Vergennes, VT).

Results and discussion

Fig. 2a shows the displacement amplitude of both the PZT surface and the membrane as a function of the input voltage to the PZT, the former measured *via* an LDV (a typical surface scan is shown in Fig. 2b) and the latter *via* visual inspection from the high speed camera images. It can be seen that despite the small nanometer amplitude vibrational displacement on the PZT surface—undetectable to the human touch, which is consistent with the limitations observed for these piezoelectric haptic actuation schemes—its coupling into the liquid within the reservoir leads to a significant amplification in the response of the membrane by approximately ten- to fifty-thousand fold, such that the 100 μm-order deflection is now well within the 100–200 μm comfortable detection range for human tactile sensation.[14,15,17] Moreover, the force produced by the membrane deflection—estimated from its mass and acceleration, which we measure as it deforms—is nearly 2 mN, which is comparable with the range required for human perception.[21,22]

Besides the static deformation, we also observe the membrane to dynamically oscillate at frequencies in the kHz range, as can be seen by the LDV measurements directly on the membrane in the inset of Fig. 2c; this is consistent with the subharmonic broadband capillary response of liquid droplets excited by MHz frequency vibrations on similar piezoelectric substrates reported elsewhere.[23] More importantly, we note that the dynamic membrane behaviour is within the sub-kHz to 1 kHz frequencies required to induce a vibrotactile sensation to touch by a human finger, especially given that the 0.5 μm displacement magnitudes observed for this frequency range are higher than the requisite 0.1 μm threshold.[24] Similar sub-kHz oscillations along the membrane can also be seen for the membrane at rest, although these arise due to noise and interference from the surrounding equipment, and are too small (around 0.5 nm) to be detected by touch.

In the absence of the TPU membrane altogether, we observe the liquid deformation to be considerably larger—several mm as can be seen in Fig. 3a. This can be attributed to the dampening effect that the membrane, with its associated stiffness, imposes on the sound energy in the liquid phase.[25] In order to minimise this effect and hence optimise the performance of the actuator, we turn to examine the effect of the membrane geometry on its deformation amplitude. Fig. 3b shows, for example, that the membrane thickness, as expected, has a considerable effect on its ability to deform—the thinner the membrane, the greater the deformation amplitude for the same input parameters—whereas the effect of the lateral dimension of the liquid chamber (as well as that of the membrane) shown in Fig. 3c and e is less intuitive, although quite revealing of the fundamental mechanisms by which the membrane deflection is coupled to the substrate vibration through the liquid.

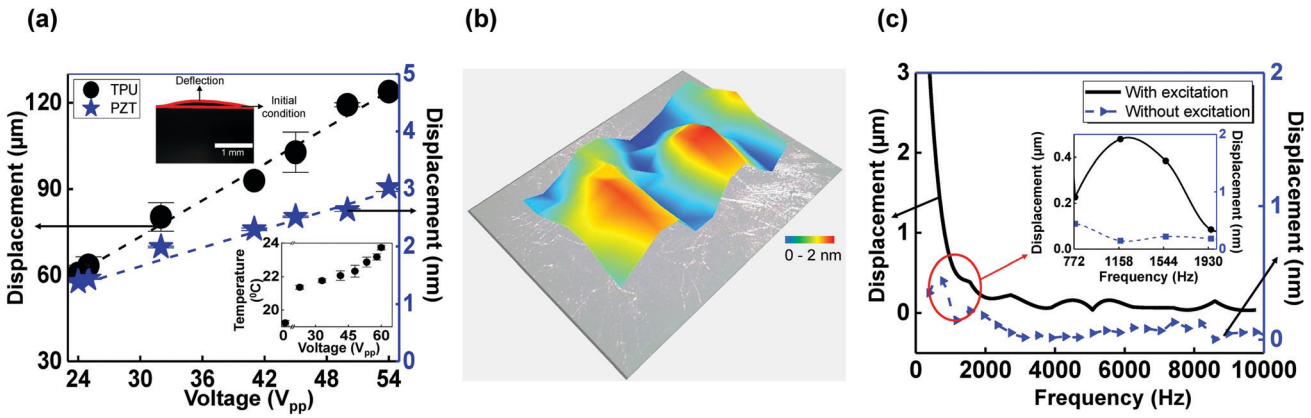

Fig. 2 (a) Nanometer-order vibration displacement amplitude along the PZT surface (★ right axis) compared to the 100 μm-order displacement in the 25 μm thick TPU membrane (■ left axis), the latter driven by the coupling of the sound energy into the liquid, as a function of the applied voltage (0.5 s pulse) to the PZT transducer. The top inset shows an image of the membrane atop a chamber prior to and upon acoustic excitation for an applied voltage of 52 V_{pp} and the bottom inset shows the temperature rise inside the chamber (4 mm-diameter) for an applied voltage over a range of 0 to 60 V_{pp}. Error bars denote the standard error in the measurements; the standard error for the PZT surface displacement amplitude is below 1% and hence is not apparent. (b) 3D LDV scan showing the surface vibration displacement on the PZT disc (3 mm × 4 mm) for an applied voltage of 24 V_{pp}. (c) Vibrational spectra of the membrane both in the absence and in the presence of the acoustic forcing. The inset shows a magnification of the displacement amplitudes in the 1 kHz frequency range, revealing appreciable displacements of around 0.5 μm under acoustic excitation—which are above the 0.1 μm detectable threshold for a human finger.

 This journal is © The Royal Society of Chemistry 2019

Published on 15 April 2019. Downloaded by RMIT University Library on 5/18/2021 12:58:18 AM.

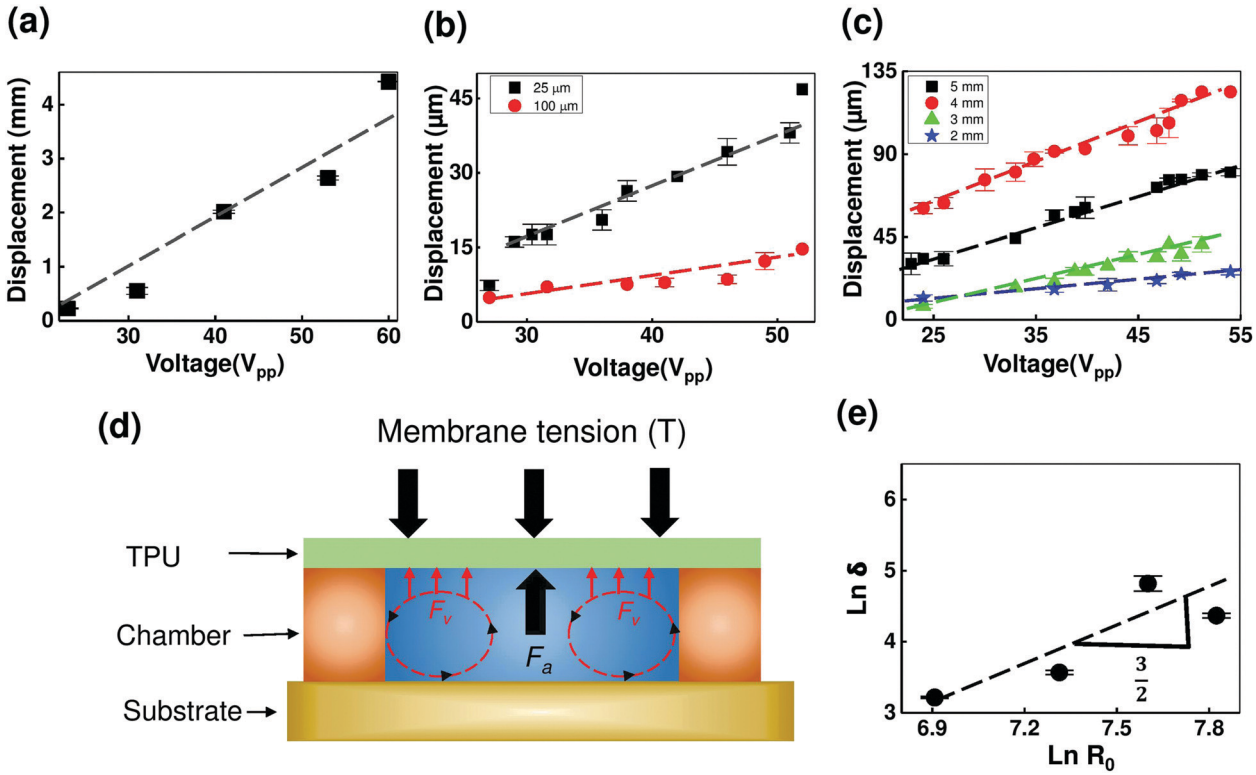

Fig. 3 (a) Displacement amplitude of the free liquid surface in the 4 mm chamber in the absence of the TPU membrane as a function of the applied voltage. Effect of (b) membrane thickness and (c) chamber diameter on the ability of the membrane to deform under an applied voltage. The chamber dimension is 3 mm in (b) and the membrane thickness is 25 μm in (c). (d) Schematic depicting the dominant forces acting on the membrane. (e) Membrane deformation amplitude δ as a function of the chamber radius R for a membrane thickness of 25 μm. In each of the experiments, the pulse duration is fixed at 0.5 s.

The dominant forces acting on the membrane are illustrated in Fig. 3d; the observation that the temperature rise in the liquid throughout the duration over which the acoustic forcing is applied is limited to under 5 °C, as shown in the inset of Fig. 2a, suggests the negligible role of heating effects in the deformation of the membrane. The acoustic radiation force F_a[26,27] and also the viscous normal stress due to the acoustic streaming in the liquid F_v, both of which are generated as a consequence of the coupling of the sound waves into the liquid due to the substrate vibration and which act to deform the membrane upwards, are balanced by the tension along the membrane T. For a thin, axisymmetric and isotropic membrane at equilibrium, assuming the deformation to be quasistatic, a dominant balance between these forces assumes the form

$$\frac{p_a}{2\delta\kappa} \sim \mu\frac{U}{R}, \tag{1}$$

where δ is the deformation of the membrane and $\kappa \sim 1/R$ is the membrane curvature. The expression on the left of the equation above comprises a generalised expression of the normal stress exerted on a membrane[28,29] that deforms under a uniform time-dependent acoustic radiation pressure $p_a \sim \rho\omega^2\xi^2$, in which ρ is the liquid density, ω is the frequency and ξ is the vibrational displacement amplitude of the substrate, whereas the expression on the right constitutes the normal viscous stress wherein μ is the liquid viscosity and U is the characteristic streaming velocity. We note the relationship above to be relatively insensitive to variation in the physical properties of the membrane and hence the exact constitutive stress–strain relationship, at least for small deformation amplitudes δ, which is not an unreasonable assumption in the present system. In order to explicate the dependence of U on R, we consider the acoustic streaming force in the fluid[30,31]

$$F_s \sim \rho\mathbf{u}\cdot\nabla\mathbf{u} \sim \rho\omega^2\xi^2\alpha\exp(-2\alpha R), \tag{2}$$

wherein $\mathbf{u}$ is the time-averaged streaming velocity field with characteristic order-of-magnitude U as the sound wave propagates through the liquid and α the attenuation coefficient of the sound wave. Given that α is typically small, it follows from eqn (2) that $U^2/R \sim 1$ or $U \sim R^{1/2}$ for constant ρ, ω and ξ. Substituting this dependence into eqn (1) wherein $\delta \sim R^2/U$ then suggests

$$\delta \sim R^2/U \sim R^{3/2}, \tag{3}$$

which is in reasonable agreement with the scaling obtained in Fig. 3e. We note that the deviation of the data from this scaling relationship could potentially arise due to the fairly rapid response of the membrane, which may not be fully compatible with the quasisteady assumption. Additionally, the membrane response can be seen to exhibit considerable hysteresis (Fig. 4a) arising due to the nonlinear ferroelectric effect inherent in PZT[32] (around 20%,[33,34] which is close to the 24% hysteresis

Published on 15 April 2019. Downloaded by RMIT University Library on 5/18/2021 12:58:18 AM.

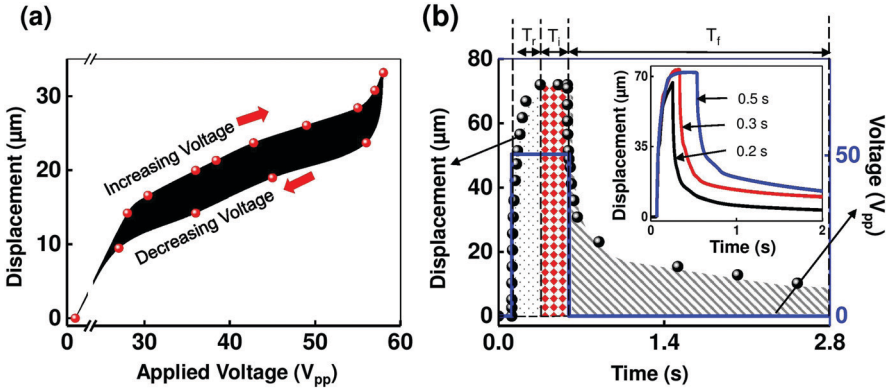

Fig. 4 (a) Membrane displacement amplitude measured through a cyclic input voltage sweep, showing the hysteresis present in the system with a 25 μm-thick TPU membrane atop a 2 mm-diameter PMMA chamber. (b) Displacement–time curve (black dots) in response to a 50 V_{pp} pulsed (0.5 s) input signal showing the characteristic rise T_r, interaction T_i and recovery T_f times. The inset graph shows the displacement–time curve for different pulse widths. In all of the cases, the data are shown for a membrane thickness of 25 μm and for a 4 mm-diameter chamber, although we observe the response to be similar.

observed), although we note that the response is approximately linear between 25 and 55 V_{pp}, which is sufficiently adequate for applications involving precision manipulation.[35]

A typical response curve of the membrane over one excitation cycle (50 V_{pp} 0.5 s pulse over a 2.8 s duration window) is shown in Fig. 4b, in which we observe the membrane to attain its full displacement amplitude within a rise time T_r of 0.16 s. In a separate experiment in which the chamber was left uncovered (*i.e.*, no membrane was present), we noticed a similar rise time for the deformation of the liquid–air interface (not shown), thus suggesting that the TPU membrane tension and the presence of the membrane itself do not appreciably alter the response dynamics despite dampening the deformation amplitude. We also note from Fig. 4b an interaction time T_i—the period over which the actuator can sustain the membrane at its maximum deformation amplitude—of 0.34 s, which we found to be proportional to the pulse width of the signal (see the inset of Fig. 4b). Following removal of the input signal, a fall time T_f of 0.3 s was required for the membrane to relax to 20% of its maximum deformation amplitude, although the period over which the membrane returned to its original state was prolonged,[36] which is not uncommon for piezoelectric materials such as PZT due to the slow changeover in the crystal domains over time following relaxation of the applied voltage, which is commonly known as piezoelectric creep.[32] Even so, we note that the current actuator performance, together with the relatively fast response time and extended interaction capacity, falls within the accepted standard required for tactile haptic actuators (0.08–40 s for relaxation to its initial state following removal of the applied voltage[32,36,37]).

To briefly show the possibility for multiplexing, and to demonstrate the possibility to localise the vibration, we diced 9 PZT elements using a wafer dicer (DAD 231; DISCO Corp., Mesa, AZ) and embedded each within a 3D printed housing arranged into a 3 × 3 array (Fig. 5a). The housing was printed (Markforged, Watertown, MA) with two small holes at the bottom to allow the vertical pins from the underlying PCB—designed to align with the array and routed to a 9 end-pin plug—to electrically contact the bottom electrode of each PZT disc. Thin wires were then soldered to the corner of the top electrode and fed through a small hole to contact one pin for each PZT. Care was taken to ensure that the soldering height did not exceed 1 mm and therefore does not protrude beyond the liquid reservoir height.

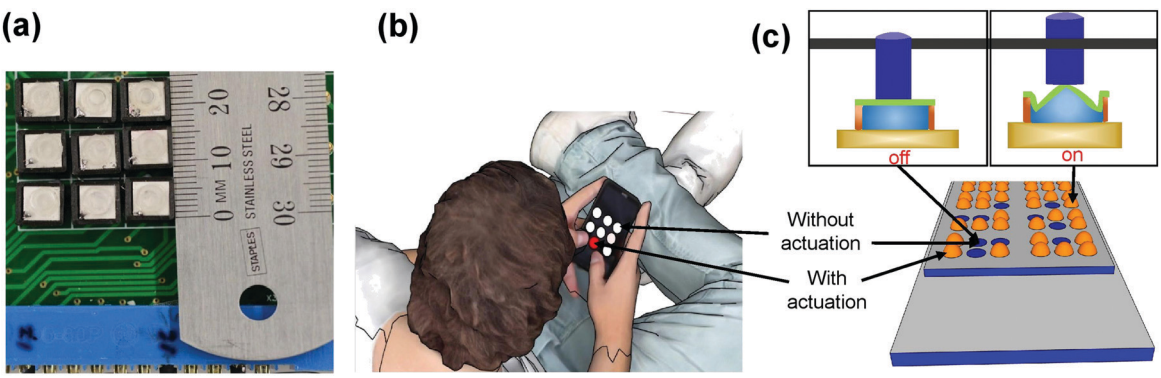

Fig. 5 (a) 3 × 3 array of PZT elements integrated with TPU-membrane-covered (25 μm-thick) PMMA chambers (3 mm-diameter), confined within 3D printed housing and electrically excited from beneath through a PCB as a proof-of-concept demonstration of the possibility of individual, sequential and simultaneous actuation for (b) mobile phone or (c) electronic braille applications.

 This journal is © The Royal Society of Chemistry 2019

Published on 15 April 2019. Downloaded by RMIT University Library on 5/18/2021 12:58:18 AM.

The soldering was also placed at the corner of the PZT to avoid any interference with the reservoir. The actuation was then performed manually with the use of 9 switches or can be programmed through an Arduino configuration connected to 9 relays to facilitate the possibility for individual, sequential or simultaneous addressability for mobile phone (Fig. 5b) or electronic braille (Fig. 5c) applications.

Conclusion

In this work, we demonstrate that the transmission of the standing wave vibration generated along a small ultrasonic transducer disc into a liquid couplant within a microfluidic chamber can give rise to both static 100 μm-order amplitude deformations and dynamic vibration in the kHz frequency range with 0.5 μm displacement amplitudes in a thermoplastic membrane atop the chamber as a potential actuation mechanism in tactile haptic feedback devices. The system therefore circumvents the limitation of small 10–100 nm order deformations that can be typically achieved with direct piezoelectric tactile haptic actuators, whilst retaining their advantages of relatively fast response times and relatively low energy input. In addition to briefly elucidating the role of the acoustic radiation pressure and viscous normal stresses arising from the acoustic streaming that are generated as a consequence of the propagation of sound waves in the liquid, we show that the miniaturisability of the setup makes it amenable for integration into parallel arrays for multiplex haptic touch operations, for example, in mobile phone and electronic braille applications.

Conflicts of interest

There are no conflicts to declare.

Acknowledgements

This work was partially carried out at the RMIT MicroNano Research Facility (MNRF), which is part of the Victorian Node of the Australian National Fabrication Facility (ANFF). LYY gratefully acknowledges funding from the Australian Research Council (ARC) through Discovery Project (DP170101061). SAMS acknowledges funding from the Iran National Institute for Medical Research Development (NIMAD) under grant number 957144.

References

1 H. Culbertson, S. B. Schorr and A. M. Okamura, Haptics: the present and future of artificial touch sensation, *Annual Review of Control, Robotics and Autonomous Systems*, 2018, **1**, 385–409.
2 V. Hayward, O. R. Astley, M. C.-H. D. Grant and G. Robles-De-La-Torre, Haptic interfaces and devices, *Sens. Rev.*, 2004, **24**, 16–29.
3 K. Takemura, S. Park and T. Maeno, Control of multi-dof ultrasonic actuator for dexterous surgical instrument, *J. Sound Vib.*, 2008, **311**, 652–666.
4 G.-Y. Yun, J. Kim, J.-H. Kim and S.-Y. Kim, Fabrication and testing of cellulose EAPap actuators for haptic application, *Sens. Actuators, A*, 2010, **164**, 68–73.
5 H.-U. Ko, H. C. Kim, J. Kim and S.-Y. Kim, Miniaturized 3 × 3 array film vibrotactile actuator made with cellulose acetate for virtual reality simulators, *Smart Mater. Struct.*, 2015, **24**, 055018.
6 S. Yun, G.-Y. Yun, K.-B. Kim, B.-W. Kang, J. Kim and S.-Y. Kim, Film-type haptic actuator made with cellulose acetate layers, *J. Intell. Mater. Syst. Struct.*, 2014, **25**, 1289–1294.
7 K. Jun, J. Kim and I.-K. Oh, An electroactive and transparent haptic interface utilizing soft elastomer actuators with silver nanowire electrodes, *Small*, 2018, **14**, 1801603.
8 T. Lu, J. Huang, C. Jordi, G. Kovacs, R. Huang, D. R. Clarke and Z. Suo, Dielectric elastomer actuators under equal-biaxial forces, uniaxial forces, and uniaxial constraint of stiff fibers, *Soft Matter*, 2012, **8**, 6167–6173.
9 M. Li, S. Luo, T. Nanayakkara, L. D. Seneviratne, P. Dasgupta and K. Althoefer, Multi-fingered haptic palpation using pneumatic feedback actuators, *Sens. Actuators, A*, 2014, **218**, 132–141.
10 H. A. Sonar and J. Paik, Soft pneumatic actuator skin with piezoelectric sensors for vibrotactile feedback, *Front. robot. AI.*, 2016, **2**, 38.
11 A. Akther, A. Kafy, L. Zhai, H. C. Kim, M. I. R. Shishir and J. Kim, Ultrasonic wave propagation of flexible piezoelectric polymer for tactile actuator: simulation and experiment, *Smart Mater. Struct.*, 2016, **25**, 115043.
12 M. Mohiuddin, K. K. Sadasivuni, S. Mun and J. Kim, Flexible cellulose acetate/graphene blueprints for vibrotactile actuator, *RSC Adv.*, 2015, **5**, 34432–34438.
13 G. Lindner, Sensors and actuators based on surface acoustic waves propagating along solid–liquid interfaces, *J. Phys. D: Appl. Phys.*, 2008, **41**, 123002.
14 C. E. Connor, S. S. Hsiao, J. R. Phillips and K. O. Johnson, Tactile roughness: neural codes that account for psychophysical magnitude estimates, *J. Neurosci.*, 1990, **10**, 3823–3836.
15 M. Hollins, S. Bensmaïa and E. Roy, Vibrotaction and texture perception, *Behav. Brain Res.*, 2002, **135**, 51–56.
16 R. Johansson and A. Vallbo, Detection of tactile stimuli. Thresholds of afferent units related to psychophysical thresholds in the human hand, *J. Physiol.*, 1979, **297**, 405–422.
17 T. Miyaoka, T. Mano and M. Ohka, Mechanisms of fine-surface-texture discrimination in human tactile sensation, *J. Acoust. Soc. Am.*, 1999, **105**, 2485–2492.
18 B. H. Ha, K. S. Lee, G. Destgeer, J. Park, J. S. Choung, J. H. Jung, J. H. Shin and H. J. Sung, Acoustothermal heating of polydimethylsiloxane microfluidic system, *Sci. Rep.*, 2015, **5**, 11851.
19 S. A. M. Shaegh, Z. Wang, S. H. Ng, R. Wu, H. T. Nguyen, L. C. Z. Chan, A. G. G. Toh and Z. Wang, Plug-and-play microvalve and micropump for rapid integration with microfluidic chips, *Microfluid. Nanofluid.*, 2015, **19**, 557–564.
20 S. A. M. Shaegh, A. Pourmand, M. Nabavinia, H. Avci, A. Tamayol, P. Mostafalu, H. B. Ghavifekr, E. N. Aghdam, M. R. Dokmeci, A. Khademhosseini and Y. S. Zhang, Rapid

Published on 15 April 2019. Downloaded by RMIT University Library on 5/18/2021 12:58:18 AM.

prototyping of whole-thermoplastic microfluidics with built-in microvalves using laser ablation and thermal fusion bonding, *Sens. Actuators, B*, 2018, **255**, 100–109.
21 H. H. King, R. Donlin and B. Hannaford, *Proceedings of the IEEE Haptics Symposium*, 2010, pp. 95–99.
22 S. Mun, S. Yun, S. Nam, S. K. Park, S. Park, B. J. Park, J. M. Lim and K.-U. Kyung, Electro-Active Polymer Based Soft Tactile Interface for Wearable Devices, *IEEE Trans. Haptics*, 2018, **11**, 15–21.
23 J. Blamey, L. Y. Yeo and J. R. Friend, Microscale capillary wave turbulence excited by high frequency vibration, *Langmuir*, 2013, **29**, 3835–3845.
24 T. Soneda and K. Nakano, Investigation of vibrotactile sensation of human fingerpads by observation of contact zones, *Tribol. Int.*, 2010, **43**, 210–217.
25 U. Ackermann, H. Fuchs and N. Rambausek, Sound absorbers of a novel membrane construction, *Appl. Acoust.*, 1988, **25**, 197–215.
26 D. Koyama, R. Isago and K. Nakamura, Compact, high-speed variable-focus liquid lens using acoustic radiation force, *Opt. Express*, 2010, **18**, 25158–25169.
27 G. Destgeer, B. Ha, J. Park and H. J. Sung, Lamb wave-based acoustic radiation force-driven particle ring formation inside a sessile droplet, *Anal. Chem.*, 2016, **88**, 3976–3981.
28 R. Hill, A theory of the plastic bulging of a metal diaphragm by lateral pressure, *Philos. Mag.*, 1950, **41**, 1133–1142.
29 G. Machado, D. Favier and G. Chagnon, Membrane curvatures and stress-strain full fields of axisymmetric bulge tests from 3D-DIC measurements. theory and validation on virtual and experimental results, *Exp. Mech.*, 2012, **52**, 865–880.
30 S. Shiokawa, Y. Matsui and T. Ueda, Study on SAW streaming and its application to fluid devices, *Jpn. J. Appl. Phys.*, 1990, **29**, 137–139.
31 J. Friend and L. Yeo, Microscale acoustofluidics: microfluidics driven via acoustics and ultrasonics, *Rev. Mod. Phys.*, 2011, **83**, 647–704.
32 R. Changhai and S. Lining, Hysteresis and creep compensation for piezoelectric actuator in open-loop operation, *Sens. Actuators, A*, 2005, **122**, 124–130.
33 C. Newcomb and I. Flinn, Improving the linearity of piezoelectric ceramic actuators, *Electron. Lett.*, 1982, **18**, 442–444.
34 P. Ge and M. Jouaneh, Modeling hysteresis in piezoceramic actuators, *Precis. Eng.*, 1995, **17**, 211–221.
35 R. Xiong, X. Liu and Z. Lai, Modeling of hysteresis in piezoelectric actuator based on segment similarity, *Micromachines*, 2015, **6**, 1805–1824.
36 T. Levard, P. J. Diglio, S.-G. Lu, C. D. Rahn and Q. Zhang, Core-free rolled actuators for Braille displays using P(VDF–TrFE–CFE), *Smart Mater. Struct.*, 2011, **21**, 012001.
37 H. Shin, J.-M. Lim, J.-U. Lee, G. Lee and K.-U. Kyung, Effect of tactile feedback for button GUI on mobile touch devices, *ETRI J.*, 2014, **36**, 979–987.

 This journal is © The Royal Society of Chemistry 2019